FISEVIER

Contents lists available at ScienceDirect

# Resources, Conservation & Recycling

journal homepage: www.elsevier.com/locate/resconrec



# Full length article



# Utilization of off-specification fly ash in preparing ultra-high-performance concrete (UHPC): Mixture design, characterization, and life-cycle assessment

Jiang Du<sup>a</sup>, Zhuo Liu<sup>a</sup>, Christos Christodoulatos<sup>a</sup>, Matthew Conway<sup>b</sup>, Yi Bao<sup>a</sup>, Weina Meng<sup>a,\*</sup>

### ARTICLE INFO

# Keywords: Carbon emission Off-specification fly ash (OSFA) Solid waste Sustainable material Ultra-high-performance concrete (UHPC)

### ABSTRACT

This paper presents feasibility and benefits of utilizing off-specification fly ash (OSFA), which would have otherwise been landfilled, in preparing ultra-high-performance concrete (UHPC). Effects of mixture design variables, including OSFA content, water-to-binder ratio, and slag content, on compressive and flexural properties of UHPC were tested. Experimental results showed that UHPC with proper combination of OSFA and slag achieved desired compressive and flexural strengths, as well as low autogenous shrinkage and leachability of heavy metals. The underlying mechanisms of property development were investigated through isothermal calorimetry, thermogravimetric analysis, and X-ray diffraction. Results indicated that use of OSFA retarded hydration reactions, but incorporation of slag effectively suppressed adverse effects of OSFA. Economic and environmental analysis showed that use of OSFA greatly reduced the life-cycle cost, carbon footprint, and embodied energy consumption of UHPC. This study develops a new avenue for valorization of OSFA and development of cost-effective and eco-friendly UHPC.

### 1. Introduction

Fly ash is a by-product produced by burning pulverized coal in electric generation power plants. Fly ash has been used to prepare cement-based construction materials such as Portland cement concrete, which is utilized in different types of engineering structures such as bridges, tunnels, buildings, and roads. In general, fly ash contains species that react with water and cement through hydraulic and/or pozzolanic reactions, which improve mechanical properties and durability of structures if concrete is well designed and prepared (Berndt, 2009; Falmata et al., 2020). Typically, fly ash has fine and round particles that improve fresh properties such as the flowability of concrete (Yu et al., 2015). According to ASTM C618 (ASTM C618-19 Standard 2019), there are two main types of fly ash that can be used to prepare cement-based materials, which are Class C and Class F fly ash. In general, Class C fly ash is more reactive than Class F fly ash with water. Both Class C and Class F fly ash are classified as specification-grade fly ash that has been well accepted by construction industries. Currently, more than 50% of concrete in the U.S. contains fly ash (Coal Combustion Products Production and Use Reports 2019). In addition to the benefits of fresh and hardened properties of concrete, in general, use of fly ash reduces material cost, carbon emissions, and embodied energy.

Despite of the long history of using fly ash, the percentage of used fly ash is limited (Fig. A1 in Appendix A) (Coal Combustion Products Production and Use Reports 2019). According to American Coal Ash Association, the U.S. produced over 29 million tons of fly ash in 2019 (Coal Combustion Products Production and Use Reports 2019), but only 58% fly ash was recycled into valuable products, leaving nearly 12 million tons of fly ash landfilled. Although the annual production of fly ash has been decreasing since 2011, due to promotion of clean energy such as natural gas, the annual production of fly ash is still high (about 30 million tons per year). More than 600 million tons of fly ash was landfilled in past 20 years. It was estimated if landfilled fly ash is mined and utilized in concrete, it will provide sufficient supply for more than 100 years (Ramme and Tharaniyil, 2014).

According to reference (Coal Combustion Products Production and Use Reports 2019), cement or cement-based materials accounted for about 80% of the used fly ash. However, only a portion of fly ash that satisfies specification requirements can be used in cement or cement-based materials. This is a main reason for the limited usage

E-mail addresses: weina.meng@stevens.edu, wmeng3@stevens.edu (W. Meng).

<sup>&</sup>lt;sup>a</sup> Department of Civil, Environmental and Ocean Engineering, Stevens Institute of Technology, Hoboken, NJ 07030, USA

b DEVCOM Armaments Center, Wharton, NJ 07885, USA

<sup>\*</sup> Corresponding author.

percentage of fly ash. Off-specification fly ash (OSFA) that does not satisfy the specification requirements is landfilled. The problem of low usage percentage of fly ash was exacerbated in recent years by the increased production of OSFA in the U.S. Due to the increasingly stringent environmental policy stipulated by the Environmental Protection Agency (EPA), many power plants have adopted new types of burners with low emission of nitrogen oxides (NO<sub>x</sub>) and sulfur oxide (SO<sub>x</sub>) (Ramme and Tharaniyil, 2014). The new types of burners reduced generation of NO<sub>x</sub>, SO<sub>x</sub>, and mercury, but significantly increased the volume ratio of carbon in fly ash, producing more OSFA. Cumulative production of OSFA imposes challenges, as the available area for landfill is shrinking in many major cities. Recycling of OSFA is relevant to the policy aspect for conservation of the environment.

In the literature, some scholars attempted to utilize OSFA in cementbased materials. Wen et al. (Wen et al., 2011) proposed to use OSFA as a stabilizer of heavy metals in a pavement base material. Naik et al. (Naik et al., 2010) and Lim et al. (Lim et al., 2017) proposed to use OSFA to produce low-strength concrete. Lo et al. (Lo et al., 2016) proposed to use OSFA to manufacture sintered lightweight aggregate, which could be potentially used to prepare concrete. The previous attempts showed that addition of OSFA in conventional concrete significantly compromised mechanical properties and durability. Compared specification-grade fly ash, there are three technical challenges for valorization of OSFA in concrete industry: (1) OSFA has limited reactivity for hydraulic and pozzolanic reactions, because OSFA has a limited percentage of reactive oxides such as CaO, SiO2, and Al2O3 while the reactivity is essential for key property development of concrete; (2) OSFA typically has a high content of carbon that absorbs air entrainer which is a chemical admixture that is used in conventional concrete to improve air content for long-term durability. Absorption of air entrainer compromises the durability (Freeman et al., 1997; Hill et al., 1997); (3) Unburned carbon has a low density and can float to the casting surface during the casting and finishing processes, producing heterogenous microstructures and an aesthetically undesired surface (Fly ash facts for highway engineers 2003).

To address these major challenges, this research aims to develop a new avenue for valorization of OSFA in concrete industry by utilizing high-volume OSFA in producing UHPC. Compared with conventional concrete and high-performance concrete, UHPC is a family of advanced concrete featuring exceptional compressive strength, ductility, and longterm durability (Du et al., 2021; Meng et al., 2017). Application in UHPC is expected to be a new and feasible technology to efficiently recycle OSFA. UHPC is designed to achieve dense microstructures with low permeability through maximizing the particle packing density and minimizing the low water-to-binder ratio (< 0.25) (Graybeal, 2005). Due to the outstanding properties, UHPC draws increasing interests in novel applications for engineering structures. For example, UHPC has been used in bridges (Aaleti et al., 2013; Alahmari et al., 2019; Voort et al., 2008), connections and joints (Graybeal, 2010; Graybeal, 2012; Qi et al., 2019; Verger-Leboeuf et al., 2017), and jackets for columns (Xie et al., 2019). The use of UHPC significantly enhanced mechanical properties and durability of structures, promoted construction efficiency, and enable design and construction of aesthetically appealing structures. However, currently, the use of UHPC is mainly limited to special structural elements, such as joints in bridges subjected to large and complicated loadings, because the upfront cost of UHPC is high. The unit cost of UHPC is more than ten times higher than that of conventional concrete. Although cost-effective UHPC has been developed in recent years through optimizing the mixture design and using supplementary cementitious materials such as fly ash (Meng et al., 2017; Yu et al., 2015), slag (Edwin et al., 2016; Meng and Khayat, 2017), and waste glass (Soliman and Tagnit-Hamou, 2016; Soliman and Tagnit-Hamou, 2017), the cost of UHPC is still high and hinders wider acceptance in structures. The use of landfilled OSFA is promising to develop cost-effective UHPC mixtures and significantly promote the application of UHPC.

This study investigates the feasibility of using OSFA to prepare UHPC for the first time. This study experimentally tests a hypothesis that OSFA can be used to partially replace cement in UHPC while possessing a high compressive strength (> 120 MPa) and self-consolidating property. The combination use of waste such as OSFA and slag for replacing high carbon emission materials such as cement is relevant to environmental and low-carbon policies. The main objectives and contributions of this research include: (1) to investigate the effects of OSFA on flowability, shrinkage, mechanical properties such as compressive and flexural strengths, and leachability of heavy metals for UHPC; (2) to develop effective strategies to improve the mechanical properties of UHPC with high-volume OSFA; and (3) to elucidate the underlying mechanisms of property development for UHPC. To this end, this study proposes a strategic combination use of OSFA and slag for replacement of cement. A total of ten mixtures were designed and tested to evaluate the effects of OSFA content, water-to-binder ratio, and slag content on key properties of UHPC. The investigated properties of UHPC included flowability, autogenous shrinkage, compressive strength, flexural behavior, and leaching of heavy metals. Hydration kinetics of UHPC mixtures were characterized through isothermal calorimetry. The hydration products were characterized through thermogravimetric analysis (TGA) and Xray diffraction (XRD). Economic and environmental impacts of using OSFA in UHPC were evaluated in terms of life-cycle cost, carbon footprint, and embodied energy. Moreover, the economic and environmental evaluation were extended by comparing with recent and relevant papers dealing with the recycling of waste materials in cement-based materials such as waste glass and rock dust (Colangelo et al., 2020; Sevim et al., 2021).

The remainder of the paper is organized as follows: Section 2 introduces the raw materials used to prepare UHPC mixtures. Section 3 introduces the experimental programs. Section 4 presents the experimental results and discussions on the results. Section 5 presents economic and environmental evaluations. Section 6 summarizes the conclusions.

### 2. Materials

# 2.1. Raw materials

Type I Portland cement was adopted. Slag from a local plant in New Jersey and OSFA from a power plant in Tennessee were employed as supplementary cementitious materials used to partially replace cement. Masonry sand was used as the fine aggregate. The chemical composition of the dry ingredients was characterized by X-ray fluorescence (XRF) and XDR, as listed in Table B1 in Appendix B.

The scanning electronic microscopy (SEM) image shows round particles and irregular particles, as shown in Fig. A2(a) in Appendix A. The OSFA has different morphology from Class C and Class F fly ash that have round particles. The particle size distribution curves of the cement, slag, OSFA, and sand are plotted in Fig. A2(b) in Appendix A.

The pozzolanic activity of OSFA was evaluated by the strength activity index and the Chapelle test. The strength activity index test was conducted in accordance with BS 3892 (Donatello et al., 2010). The control mortar cubes were prepared by mixing 1350 g sand, 450 g cement, and 225 ml water. To prepare the test mortar cubes, 20% cement was replaced using the OSFA. The strength activity index is the compressive strength ratio of the test samples and control samples. The strength activity indices were 0.70 at 7 days (d) and 0.73 at 28 d, as shown in Fig. A3 in Appendix A. The Chapelle test was conducted in accordance with NF P18-513 (Ferraz et al., 2015). The consumption of Ca(OH)<sub>2</sub> by 1 g OSFA was quantified. The suspension of 1 g OSFA, 1 g CaO, and 250 mL distilled water was boiled at 90 °C for 16 h (h) of continuous stirring. The unconsumed Ca(OH)2 content (free in solution) was quantified by acid titration. The pozzolanic activity of OSFA was expressed as 353.1 mg Ca(OH)2 / g OSFA. In comparison, the 28 d strength activity index is 0.80 and the Chapelle test result is 436 mg Ca

**Table 1**Mixture proportions of UHPC (kg/m<sup>3</sup>).

Mixture	Cement	OSFA	Slag	Sand	HRWR	Water	Steel fiber	Note
Control	1133.1	0	0	953.2	5.8	260.8	156.0	7.6
OSFA10	1034.6	52.9	0	967.1	5.6	250.0	156.0	7.1
OSFA20	933.2	107.4	0	981.4	5.6	239.4	156.0	6.8
OSFA30	828.8	163.5	0	996.1	5.5	228.2	156.0	6.2
OSFA20-21	953.5	109.7	0	1002.7	6.5	224.9	156.0	8.2
OSFA20-19	974.6	112.2	0	1024.9	8.0	210.6	156.0	9.3
OSFA20SL20	703.0	107.9	215.7	985.7	4.3	235.7	156.0	5.4
OSFA20SL30	587.1	108.1	324.3	987.8	4.3	234.0	156.0	5.1
OSFA20SL40	470.7	108.3	433.3	990.0	4.2	232.4	156.0	4.9
OSFA20SL60	236.4	108.8	652.9	994.3	4.2	229.0	156.0	4.8

Note: The saturation dosages of HRWR are listed for comparison with the HRWR contents.

**Table B1**Chemical and physical properties of raw materials.

	Type I Portland cement	Slag	OSFA	Sand
SiO <sub>2</sub> (%)	22.44	36.21	16.72	86.50
Al <sub>2</sub> O <sub>3</sub> (%)	2.76	11.10	10.18	0.39
Fe <sub>2</sub> O <sub>3</sub> (%)	2.24	0.76	6.66	1.47
CaO (%)	68.05	43.75	2.41	9.42
MgO (%)	0.91	5.09	0.90	_
SO <sub>3</sub> (%)	2.25	2.21	3.89	_
Na <sub>2</sub> O (%)	0.19	0.23	0.25	_
K <sub>2</sub> O (%)	0.11	0.40	1.24	_
TiO <sub>2</sub> (%)	0.14	0.58	0.49	_
P <sub>2</sub> O <sub>5</sub> (%)	0.09	0.02	0.30	_
Mn <sub>2</sub> O <sub>3</sub> (%)	0.03	0.36	0.01	_
SrO (%)	_	0.10	_	_
C <sub>3</sub> S (%)	62.35	_	_	_
C <sub>2</sub> S (%)	20.28	_	_	_
C <sub>3</sub> A (%)	1.42	_	_	_
C <sub>4</sub> AF (%)	5.83	_	_	_
Loss on ignition (%)	1.28	0.72	49.8	0.24
Specific gravity, SSD	3.15	2.90	1.45	2.64

 $(OH)_2$  / g fly ash for specification-grade fly ash, respectively, in compliance with ASTM C618 (ASTM C618-19 2019), as reported in references (De Medeiros et al., 2017; Donatello et al., 2010). The results consistently indicate that the OSFA has lower pozzolanic reactivity than the specification-grade fly ash.

According to ASTM C618 (Yu et al., 2015), the upper limit of loss on ignition of Class C and Class F is 6%, which is much lower than the loss on ignition (49.8%) of the OSFA in this study. To evaluate the loss on ignition, this research performed a TGA using a thermogravimetric analyzer (model: TA® TG55). During the test, air was input to a chamber of the TGA analyzed with OSFA sample at a constant flow rate of 50 ml/min. The TGA test results are shown in Fig. A4(a) in Appendix A. As temperature was increased from 20  $^{\circ}\text{C}$  to 1000  $^{\circ}\text{C}$  , the mass loss of OSFA sample was increased from 0 to 49.8%. The mass loss is mainly attributed to presence of elemental carbon and gypsum in the OSFA. After the TGA test, a combustion test was conducted to characterize the carbon content. It was found that elemental carbon accounted for 41.8% of the mass of OSFA, which is 84% of the loss on ignition of the OSFA. The remaining 16% of loss of ignition can be attributed to partial decomposition of gypsum at elevated temperatures, as described in references (Scrivener et al., 2018; Van der Merwe et al., 1999). The XRD results are shown in Fig. A4(b) in Appendix A. The main minerals of OSFA include gypsum, quartz, and hematite. The mass percentages of gypsum, quartz, and hematite were 51.7%, 3.2%, and 45.1%.

## 2.2. Mixture design

Table 1 lists the ten mixtures investigated in this study. The mixtures were designed based on a cost-effective UHPC developed in previous research (Fly ash facts for highway engineers 2003). Three important mix design variables were studied, which are the OSFA content (10%,

20%, and 30%, by volume of binder), water-to-binder ratio (0.23, 0.21, and 0.19, by mass), and slag content (20%, 30%, 40%, and 60%, by volume of binder). The binder-to-sand ratio was fixed at 1:1, by volume.

A polycarboxylate-based high-range water reducer (HRWR) was used to improve the flowability of the mixtures. The solid content and specific gravity of the HRWR are 34.4% and 1.05, respectively. The HRWR contents of the investigated mixtures were adjusted to ensure that the mixtures were self-flowable. Meanwhile, appropriate rheological properties such as plastic viscosity are essential to achieve appropriate fiber dispersion and orientation, as elaborated in references (Teng et al., 2020; Xie et al., 2019). To enhance the crack resistance and toughness, chopped steel fibers measuring 0.2 mm in diameter and 13 mm in length were incorporated. The tensile strength and modulus of elasticity of the steel fibers are 1.9 GPa and 203 GPa, respectively.

# 3. Experimental methods

### 3.1. Mixing and specimen preparation

A mixer (model: Hobart® HL-200) with a volume capacity of 19 L was used to mix raw materials for preparation of the mixtures. A mixing procedure developed in previous research was adopted in this study. The mixing procedure includes four main steps: (1) Step 1: The dry ingredients (cement, slag, OSFA, and sand) are introduced to the mixer and mixed at 1 rps for 2 min (min); (2) Step 2: The HRWR is dissolved in the mixing water to form a solution, and 90% of the solution is introduced to the mixer and mixed at 1 rps for 3 min; (3) Step 3: The rest of solution is added, and the mixture is mixed at 2 rps for 3 min; (4) Step 4: The steel fibers are added to the mixer and mixed at 2 rps for 2 min. After mixing, the mixtures were examined by hand, and no fiber agglomeration or segregation was found.

The mixtures were used to cast three types of specimens, which are cubic specimens for compressive test, beam specimens for flexural test, and tube specimens for shrinkage test. More details of the specimens are introduced in the following sections. During casting, although the mixtures were self-flowable, the molds were placed on a vibration table to ensure a high casting quality. Immediately after casting, the specimens were covered by wet burlap and plastic sheet. The specimens were demolded after 1 d, and then cured in lime-saturated water at room temperature (23  $\pm$  2  $^{\circ}\text{C}$ ) until testing.

### 3.2. Fresh and hardened properties

The flowability of the investigated mixtures was evaluated through mini-slump flow test, in accordance with ASTM C230 (ASTM C230 2021). The mini-slump flow test was used to adjust the HRWR content to secure self-consolidating property of the mixtures.

The compressive strength was evaluated through uniaxial compressive tests using 50 mm cubes, in accordance with ASTM C109 (ASTM C109 /C109M-20b 2020). The loading rate was kept constant at 1.8 kN/min. The compressive tests were conducted at 1, 3, 7, 14, and 28 d

The flexural properties were evaluated through four-point bending tests in according with ASTM C1609 (ASTM C1609 /C1609M-19a 2019). The test specimens measured 280 mm  $\times$  76 mm  $\times$  13 mm. The loading span length was 94 mm. The bending tests were conducted using a load frame (model: Instron® 5982) under displacement control. The displacement rate was 0.05 mm/min. The tests were performed to evaluate the flexural strength and energy dissipation at 7 d and 28 d The flexural strength was calculated using Eq. (1)

$$\sigma = \frac{3F(L - L_i)}{2bd^2} \tag{1}$$

where F, L,  $L_b$  b, and d are the peak load, distance between supports (L = 240 mm), distance between loads ( $L_i$  = 94 mm), beam width, and beam depth, respectively. The area between the load-deflection curve and horizontal axis (from 0 to L/40) is the energy dissipation capability.

### 3.3. Hydration heat

The heat of hydration of each mixture was evaluated using an isothermal calorimeter (model: Calmetrix® I-Cal 4000 HPC), which was programmed to maintain the sample at 25 °C. About 60 g of fresh mixture was sealed in a plastic vial and placed in the calorimeter. The heat of hydration was continuously measured from 2 min after completion of mixing until 48 h. The results were normalized by the mass of binder.

### 3.4. Autogenous shrinkage

The autogenous shrinkage was evaluated according to ASTM C1698 (ASTM C1698-19 2019). Due to the low water-to-binder ratio, UHPC features large autogenous shrinkage, which may cause cracks and debonding in structures, as elaborated in references (Holt and Leivo, 2004; Yoo et al., 2014). Cracks and debonding can highly compromise the mechanical properties and durability of structures. This research evaluated the autogenous shrinkage of the investigated UHPC mixtures using tube specimens (ASTM C1609 /C1609M-19a 2019). The specimens were cast in corrugated plastic tubes and stored at a constant temperature (23 °C  $\pm$  1 °C) and relative humidity (50%  $\pm$  1%). Length change of the specimens was measured and used to calculate the autogenous shrinkage. The first measurement was carried out at 12 h after casting, then on a daily basis for the first week, and finally on a weekly basis until 28 d

### 3.5. Thermogravimetry analysis

Thermogravimetric analysis was carried out using a thermal analyzer (model: TA® TG55) to evaluate the hydration kinetics of the mixtures. For the sample preparation, 50 mg of samples from dried slices (after stopping hydration with isopropanol) was crushed into fine powders and vacuum dried 24 h before the test. During the test, the sample was heated at a constant rate of 20 °C/min from 20 °C to 1000 °C in a 50 ml/min flow of nitrogen.

# 3.6. X-ray diffraction

X-ray diffraction test was carried out using a diffractometer (model: Panalytical X' pert Pro) to evaluate the hydration products of the mixtures. The sample preparation was the same as that in the TGA test. During the XRD test, powder samples were scanned on a rotating stage between  $5^{\circ}$  and  $65^{\circ}(2\theta)$  using an X'Celerator detector. The step size of scanning was  $0.0167^{\circ}$  ( $2\theta$ ), and the time per step was 30 s.

# 3.7. Leaching of heavy metals

Leaching of heavy metals from OSFA and UHPC was evaluated by

 Table B2

 Heavy metal contents and allowable leaching limits in TCLP test.

Heavy metals	As	Pb	Se
OSFA	518	116	360
Allowable leaching limits (Holt and Leivo, 2004)	ppm 5 ppm	ppm 5 ppm	ppm 1 ppm

toxicity characteristic leach procedure (TCLP) tests and compared with regulatory limitations. Sample solutions were prepared using OSFA powder and crushed UHPC, in accordance with reference (EPA, 1992), with a liquid-to-solid ratio of 20. The samples were stored in polyethylene bottles tumbled at a speed of 30 rpm for 18 h and then vacuum filtered using 0.6  $\mu m$  to 0.8  $\mu m$  glass fiber filters. The filtered samples were collected for measuring heavy metal ions using inductively coupled plasma-optical emission spectrometry (ICP-OES). Heavy metals arsenic (As), lead (Pb), and selenium (Se) in the OSFA were higher than the allowable limits, as shown in Table B2 in Appendix B. Thus, leachability of the UHPC mixtures was investigated in this research.

### 4. Experimental results and discussion

### 4.1. Flowability

The effect of OSFA on flowability of the mixtures was evaluated by mini-slump flow test. First, the HRWR content was fixed at 0.52% by mass of binder. As the OSFA content increased from 0 to 30%, the mini-slump spread was increased from 230 mm to 290 mm (by 26%), as shown in Fig. A5(a) in Appendix A. The results indicated that the addition of OSFA improved the workability of UHPC which is attributed to the finer particles of the OSFA compared with cement particles.

Then, the mini-slump spread was controlled at 280  $\pm$  20 mm for the rest of mixtures by adjusting the HRWR content to achieve selfconsolidation. For example, as the water-to-binder ratio decreased from 0.23 to 0.19, the HRWR demand was increased from 0.53% to 0.73%, consistent with reference (Fly ash facts for highway engineers 2003). As the slag content increased from 0 to 60%, the HRWR demand was sustained at a low level. The saturation dosage of superplasticizer or HRWR was evaluated by mini-slump flow tests according to ASTM C230 (ASTM C230 2021). The results of the saturation dosage of HRWR are listed in Table 1. The HRWR content of each mixture was lower than the saturation dosage, as shown in Fig. A5(b). The HRWR content was controlled to achieve desired flowability while preventing segregation. When the HRWR content is too high, the viscosity of the UHPC will be too low to homogenize the raw materials. Specifically, the OSFA with low density will float to the top surface, and the steel fibers with high density will sink to the bottom. The optimal HRWR content was determined to achieve appropriate plastic viscosity, as elaborated in reference (Xie et al., 2019). Throughout the flowability tests of the investigated UHPC mixtures, no segregation was observed. The desired flowability is attributed to the appropriate plastic viscosity of the mixtures.

### 4.2. Compressive strength

Fig. 1 plots the results of compressive strengths of the mixtures from 1 d to 28 d The columns represent the average results of three specimens. The error bars show the standard deviations. Fig. 1(a) shows the effects of OSFA content and water-to-binder ratio on the compressive strength. Fig. 1(b) shows the effect of slag content on the compressive strength.

In Fig. 1(a), as the OSFA content increased from 0 to 30% by volume of binder, the compressive strength at 1 d was reduced from 73.4 MPa to 5.2 MPa (by 93%), and the compressive strength at 28 d was reduced from 104.7 MPa to 77.1 MPa (by 26%), meaning that addition of OSFA reduced compressive strengths, especially at early ages. It is speculated

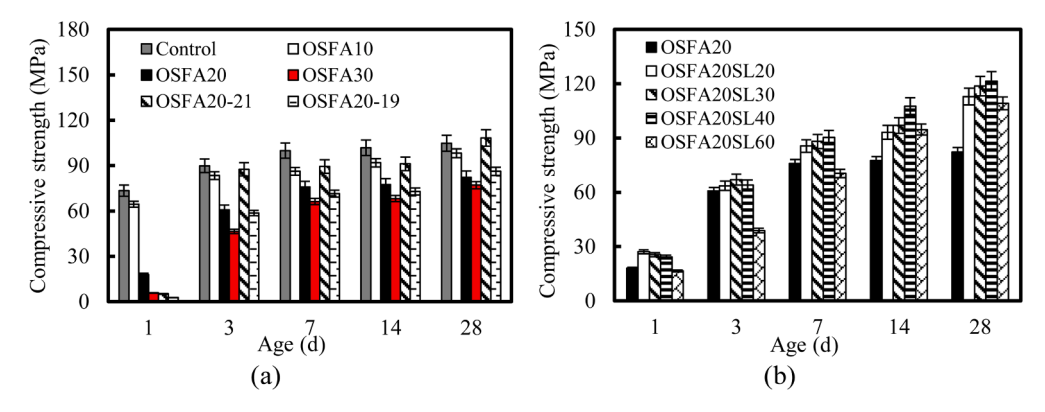


Fig. 1. Compressive strength results: (a) OSFA content and water-to-binder ratio; (b) slag content.

that the OSFA has a low reactivity in hydration. The speculation is tested by the measurement of hydration heat using the isothermal calorimeter. The results are elaborated in Section 4.5.

As the water-to-binder ratio decreased from 0.23 (OSFA20) to 0.19 (OSFA20-19), the compressive strength at 1 d was reduced from 18.0 MPa to 2.8 MPa (by 84%). The reduction of compressive strength is attributed to the increase of HRWR content (Table 1), because HRWR retards hydration reactions at early ages (Li et al., 2017). This explanation is corroborated by the measurement of hydration heat (Section 4.5). The compressive strength of OSFA20-21 was the highest among the three mixtures at 28 d The compressive strength of OSFA20-21 was higher than that of OSFA20, because the water-to-binder ratio of OSFA20-21 was lower than that of OSFA20. A low water-to-binder ratio tends to densify the microstructure and thus increase the compressive strength. The compressive strength of OSFA20-21 was higher than that of OSFA20-19. This is attributed to the higher HRWR content of OSFA20-19. In summary, the compressive strength is a result of the competition effects of the HRWR content and water-to-binder ratio on the hydration reactions and microstructures.

In Fig. 1(b), as the slag content increased from 20% to 60%, the highest compressive strength was achieved by different mixtures at different ages: OSFA20SL20 achieved the highest strength at 1 d; OSFA20SL30 achieved the highest strength at 3 d; and OSFA20SL40 achieved the highest strength at 7 to 28 d The results indicate that proper use of slag can increase the compressive strength and show a trend that the optimal slag content increases with the age of mixture. It is speculated that the slag can promote the hydration and pozzolanic reactions but use of an excessive amount of slag can compromise the hydration reactions and microstructure. Since pozzolanic reactions are slower than hydration reactions in general, a higher increase of compressive strength is expected to occur at later ages, consistent with the test results in Fig. 1(b). It should be noted that mixture OSFA20SL40 achieved a compressive strength of 121.5 MPa at 28 d The speculation of the underlying mechanism is further investigated through measurement of hydration heat, XRD test, and TGA test.

### 4.3. Flexural properties

Fig. 2 plots the flexural test results at 7 d and 28 d All of the investigated mixtures demonstrated desired ductility. The beams resisted higher loads after they were cracked. Fig. 2(a) and Fig. 2(b) show the effect of OSFA content. Fig. 2(c) and Fig. 2(d) show the effect of water-to-binder ratio. Fig. 2(e) and Fig. 2(f) show the effect of slag content. For each case, tests of three specimens were duplicated, and their results were averaged. The representative load-deflection curves are plotted in Fig. 2(a), Fig. 2(c), and Fig. 2(e). The average results of flexural strengths and standard deviations are plotted in Fig. 2(b), Fig. 2(d), and Fig. 2(f).

As the OSFA content increased from 0 to 30%, the flexural strength

was reduced from 24.9 MPa to 16.0 MPa (by 35%) at 7 d and from 27.5 MPa to 17.6 MPa (by 36%) at 28 d The toughness was reduced from 7.1 kNmm to 3.9 kNmm (by 45%) at 7 d and from 7.8 kNmm to 5.0 kNmm (by 38%) at 28 d As the water-to-binder ratio decreased from 0.23 to 0.19, the highest flexural strength and toughness were achieved by mixture OSFA20–21 with a water-to-binder ratio of 0.21. At 28 d, the flexural strength of OSFA20–21 was 7% higher than that of OSFA20 and 8% higher than that of OSFA20–19; and the toughness of OSFA20–21 was 13% higher than that of OSFA20 and 15% higher than that of OSFA20–19.

As the slag content increased from 20% to 60%, the highest flexural strength and toughness were achieved by mixture OSFA20SL40 with a slag content of 40%. At 28 d, the flexural strength of OSFA20SL40 was 11% higher than that of OSFA20 and 27% higher than that of OSFA20SL60; and the toughness of OSFA20SL40 was 6% higher than that of OSFA20 and 26% higher than that of OSFA20SL60. The change trends of flexural strength and toughness are consistent with the trends of compressive strength of the mixtures at 28 d

### 4.4. Autogenous shrinkage

Fig. 3 plots the results of autogenous shrinkage of the investigated mixtures. Fig. 3(a) shows the effects of OSFA content and water-to-binder ratio on autogenous shrinkage. Fig. 3(b) shows the effect of slag content on autogenous shrinkage.

As the OSFA content increased from 0 to 30%, the autogenous shrinkage at 28 d was reduced from 1089  $\mu\epsilon$  to 593  $\mu\epsilon$  (by 46%). The reduction of autogenous shrinkage can be attributed to the low reactivity of OSFA as speculated in Section 4.2. As the water-to-binder ratio decreased from 0.23 to 0.19, OSFA20–21 achieved the highest autogenous shrinkage at 28 d The autogenous shrinkage of OSFA20–21 was 7% higher than that of OSFA20 and 19% higher than that of OSFA20–19. In general, a low water-to-binder ratio leads to high autogenous shrinkage (Yang et al., 2019). However, an excessive amount of HRWR in OSFA20–19 could highly hinder the hydration reactions and thus reduce autogenous shrinkage. As the slag content increased from 0 to 60%, autogenous shrinkage at 28 d was reduced from 859  $\mu\epsilon$  to 662  $\mu\epsilon$  (by 23%). The reduction of autogenous shrinkage is because the slag is less reactive compared with the cement in terms of hydraulic reactions at the early ages (Ghafari et al., 2016).

# 4.5. Hydration heat

The isothermal calorimetry results were shown in Fig. A6 in Appendix A. Fig. A6(a) shows the effects of OSFA content and water-to-binder ratio on hydration kinetics. As the OSFA content increased from 0 to 30%, the dormant period was extended from 7 h to 25 h, and the peak of heat flow was reduced from 3.1 mW/g to 2.2 mW/g, indicating that the OSFA retarded hydraulic reactions. As the water-to-

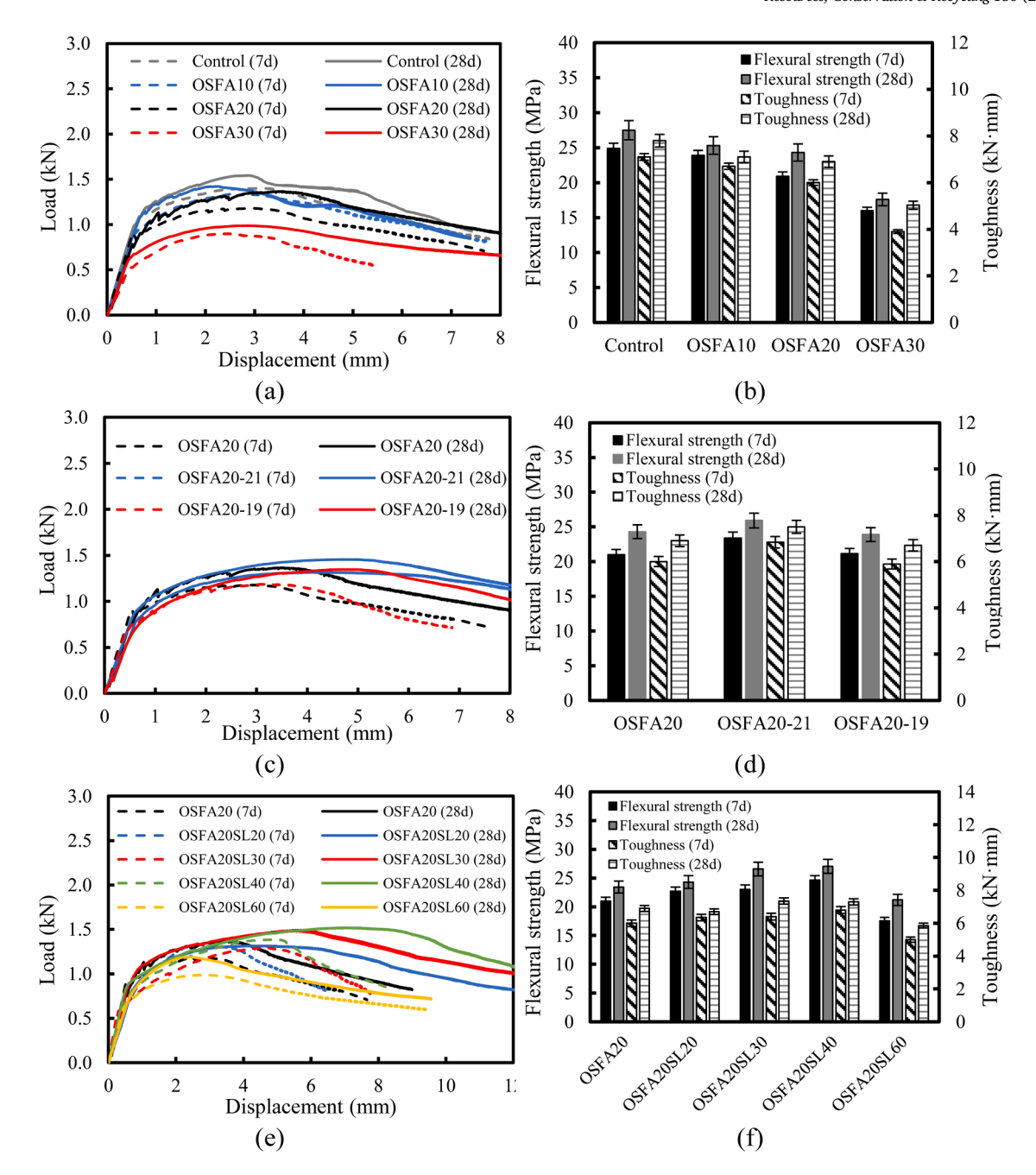


Fig. 2. Flexural test results: (a) load-displacement curves for different OSFA contents; (b) flexural strength and toughness for different OSFA contents; (c) load-displacement curves for different water-to-binder ratios; (d) flexural strength and toughness for different water-to-binder ratios; (e) load-displacement curves for different slag contents; and (f) flexural strength and toughness for different slag contents.

binder ratio decreased from 0.23 to 0.19, the dormant period was increased from 17 h to 21 h, and the peak of heat flow was reduced from 2.7 mW/g to 2.4 mW/g. The reduction of peak heat flow is attributed to the increase of HRWR content, which covers cement particles and retards hydration (EPA, 1992). Fig. A6(b) shows the effect of the slag content on the hydration kinetics. As the slag content increased from 0 to 20%, the dormant period decreased from 17 h to 9 h, and the peak heat flow was reduced from 2.7 mW/g to 2.6 mW/g. The acceleration of hydration is attributed to the reduced HRWR content (by 23%), and the reduced peak is due to the reduced cement content. As the slag content increased from 20% to 60%, the hydration reactions were hindered due to reduction of cement content. These results validated the speculations in Section 4.2.

# 4.6. Thermogravimetry analysis

Fig. 4 shows the results of TGA tests using specimens cured for 28 d Fig. 4(a) shows the effects of OSFA content and water-to-binder ratio on mass loss. Fig. 4(b) shows the effect of slag content on mass loss. Fig. 4(c) shows the effects of OSFA content and water-to-binder ratio on mass loss rate. Fig. 4(d) shows the effect of slag content on mass loss rate. Fig. 4(e) shows the bounded water content. Fig. 4(f) shows the content of calcium hydroxide (CH).

The mass loss rate is represented by derivative thermogravimetry (DTG), which is the derivative of mass loss regarding to temperature change. Each DTG curve showed three major peaks respectively corresponding to: (1) the dehydration of calcium silicate hydrates (C-S-H), ettringite, and AFm phases, up to  $400\,^{\circ}$ C; (2) the dehydroxylation of CH,

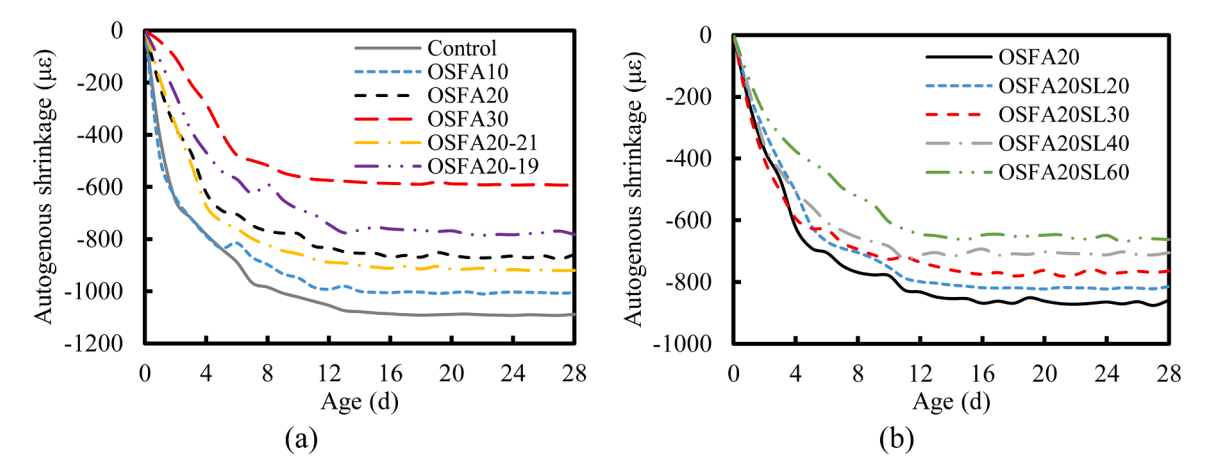


Fig. 3. Autogenous shrinkage results of investigated UHPC mixtures: (a) OSFA content and w/b effect; and (b) slag content effect.

from 400  $^{\circ}$ C to 500  $^{\circ}$ C; and (3) the decarbonation of calcium carbonate, from 500  $^{\circ}$ C to 800  $^{\circ}$ C (Huang et al., 2017).

As the OSFA content increased from 0 to 30%, the bounded water and CH contents normalized per 100-gram mortar were reduced by 12% and 9.5%, respectively, indicating that less hydration products such as C-S-H and CH were produced. Such results are consistent with the results of hydration heat and mechanical properties such as compressive strength and flexural properties. The results further validate the speculations in Section 4.2.

As the water-to-binder ratio decreased from 0.23 to 0.19, the bounded water and CH contents were reduced by 25% and 24%, respectively. This is attributed to the reduced hydration degree because the water content 0.23 is insufficient to consume the cementitious materials in the mixture (Brouwers, 2004; Brouwers, 2005). As the slag content increased from 20% to 60%, the bounded water content was increased by 21%, while the CH content was reduced by 15% This was because the slag had amorphous silica that could react with CH and produce calcium silicate hydrates through pozzolanic reactions, as discussed in reference (Falmata et al., 2020).

# 4.7. X-ray diffraction

The XRD test results of mixtures OSFA20 and OSFA20SL40 are shown in Fig. A7 in Appendix A. The crystal phases of mixtures mainly included quartz, CH, ettringite, and unhydrated cement clinkers. The characteristic peaks of ettringite include  $2\theta=9.8^{\circ}, 32.5^{\circ},$  and  $54.8^{\circ}$  The characteristic peaks of CH include  $2\theta=18.0^{\circ}, 34.1^{\circ},$  and  $36.5^{\circ}$  The characteristic peaks of quartz include  $2\theta=21.1^{\circ}, 26.6^{\circ}, 36.5^{\circ}, 39.7^{\circ},$   $50.4^{\circ},$  and  $60.1^{\circ}$  The characteristic peaks of unhydrated cement clinkers include  $2\theta=29.5^{\circ}, 41.2^{\circ}, 51.3^{\circ},$  and  $60.2^{\circ}$  As the slag content increased from 0 to 40%, the mixture OSFA20SL40 showed a lower intensity at  $2\theta=18.0^{\circ}, 34.1^{\circ},$  and  $36.5^{\circ},$  which correspond to CH, indicating that the addition of slag promoted pozzolanic reaction that consumed CH and produced C—S—-H. Such results are consistent with the results of TGA, thus validating speculations in Section 4.2.

# 4.8. Leaching of heavy metals

The results of the leaching tests are listed in Table B3 in Appendix B. The concentrations of As, Pb, and Se leached from the OSFA and crushed UHPC are lower than the allowable upper limits, indicating the leaching resistance of the UHPC mixtures satisfies requirements (Scrivener et al., 2018). The concentrations of the heavy metals of UHPC mixtures are lower than those of OSFA powder, meaning that the UHPC mixtures helps immobilize the heavy metals.

### 5. Economic and environmental benefits

Recent data (Cetin et al., 2012) indicated that landfill was the main method to dispose OSFA, which is a potential pollutant to soil and groundwater. Utilization of OSFA in UHPC provides a new avenue to valorize and upcycle solid waste for valuable products. This section assess the life-cycle cost, carbon footprint, and embodied energy consumption of UHPC with the OSFA.

### 5.1. Inventory data

The unit cost, carbon footprint, and embodied energy of the raw material ingredients according to references (Chiaia et al., 2014; Long et al., 2015; Wille and Boisvert-Cotulio, 2015) are summarized in Table B4 in Appendix B. It is worth noting that the cost, carbon emission, and embodied energy of OSFA are assumed to be zero, because OSFA have been landfilled as a solid waste. In this sense, utilizing OSFA in UHPC reduces cost, carbon emission, and energy consumption. To be conservative, those benefits are not considered in this study.

## 5.2. Economical evaluation

With the inventory data in Table B4, the unit material cost of each mixture can be calculated using Eq. (2):

$$M = \sum_{i=1}^{n} m_i r_i \tag{2}$$

where M is the unit cost of a mixture per cubic meter (unit:  $\$/m^3$ );  $m_i$  is the unit cost (unit: \$/kg) of the i th ingredient of the mixture (i = 1, 2, 3, ..., n, and n = 7), as listed in Table B4; and  $r_i$  is the mass of the i th ingredient of the mixture (unit:  $kg/m^3$ ), as listed in Table 1.

According to Eq. (2), the unit cost of each mixture was calculated. With the compressive strength (MPa) of each mixture at 28 d, the strength-normalized cost (\$/m³/MPa) was calculated. Fig. A8 in Appendix A plots the results of the results of the unit cost and strength-normalized cost of the mixtures. As the OSFA content increased from 0 to 30%, the unit cost was reduced from \$ 954 to \$ 917, and the strength-normalized cost was increased from 9.1 \$/m³/MPa to 11.9 \$/m³/MPa, because the use of OSFA reduced the compressive strength. As the water-to-binder ratio decreased from 0.23 to 0.19, the unit cost was increased from \$ 954 to \$ 963, while the strength-normalized cost was first reduced and then increased. OSFA20–21 achieved the lowest strength-normalized cost, because OSFA20–21 had a high compressive strength. As the slag content increased from 0 to 60%, the unit cost was reduced from \$ 930 to \$ 902, while the strength-normalized cost was sustained at a low value (7.5–8.2 \$/m³/MPa). Compared with the

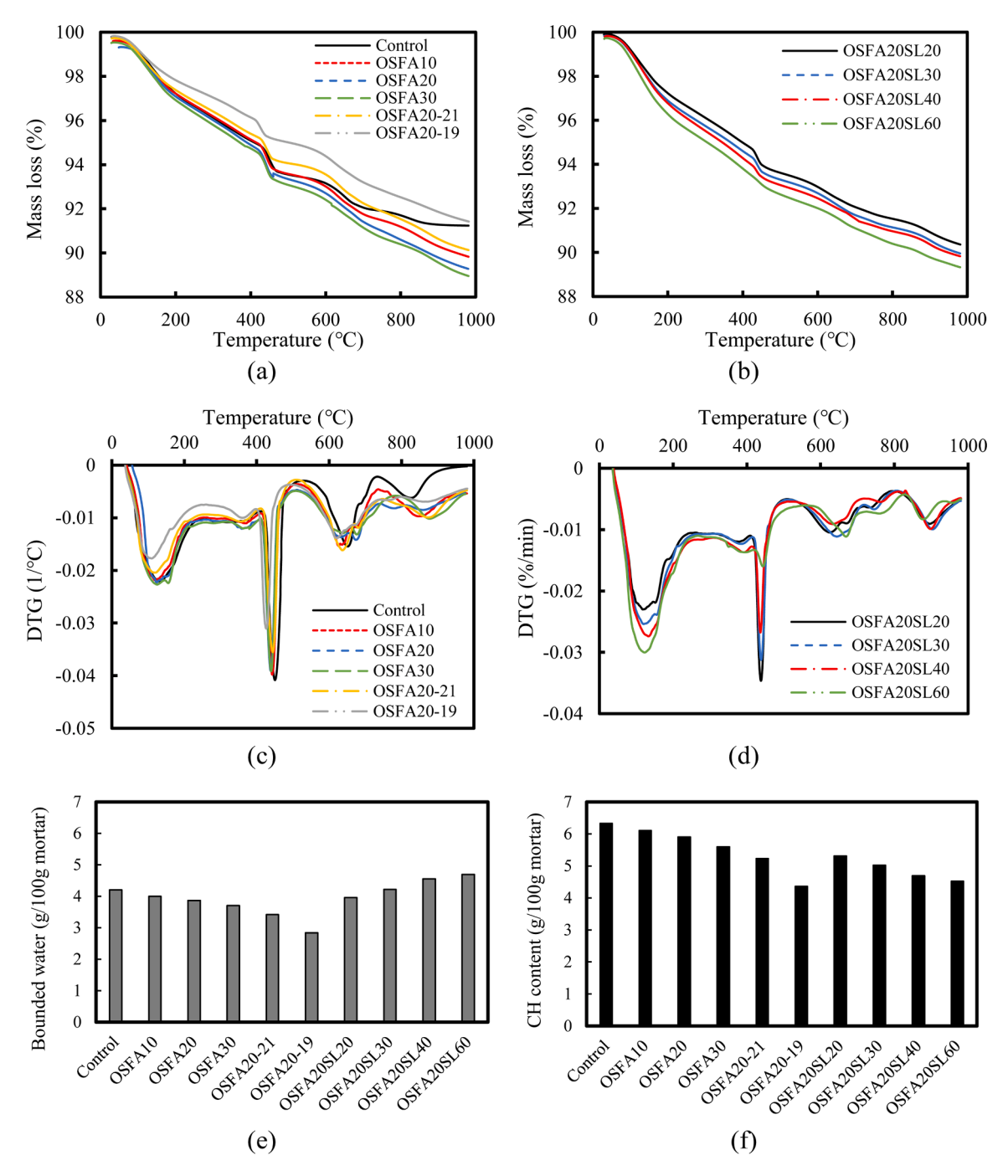


Fig. 4. Results of TGA tests: (a) effects of OSFA content and water-to-binder ratio on mass loss; (b) effect of slag content on mass loss; (c) effects of OSFA content and water-to-binder ratio on mass loss rate; (d) effect of slag content on mass loss rate; (e) bounded water content; and (f) CH content.

**Table B3**Results of TCLP.

Heavy metals	As	Pb	Se
OSFA powder	0.78 ppm	< 0.1 ppm	0.22 ppm
OSFA20	< 0.1 ppm	< 0.1 ppm	< 0.1 ppm
OSFA20-21	< 0.1 ppm	< 0.1 ppm	< 0.1 ppm
OSFA20SL40	< 0.1 ppm	< 0.1 ppm	< 0.1  ppm
OSFA20SL60	< 0.1 ppm	< 0.1 ppm	< 0.1  ppm
Allowable limitations	5 ppm	5 ppm	1 ppm

**Table B4**Inventory of unit cost, carbon footprint, and embodied energy of raw materials.

No.	Ingredient	Cost (\$/kg)	Carbon emission (kg/kg)	Embodied energy (MJ/kg)
1	Cement	0.11	0.83	4.73
2	OSFA	0.00	0.00	0.00
3	Slag	0.10	0.02	1.59
4	Sand	0.02	0.01	0.11
5	HRWR	3.60	0.72	18.30
6	Water	0.00	0.00	0.01
7	Steel fiber	4.76	1.49	20.56

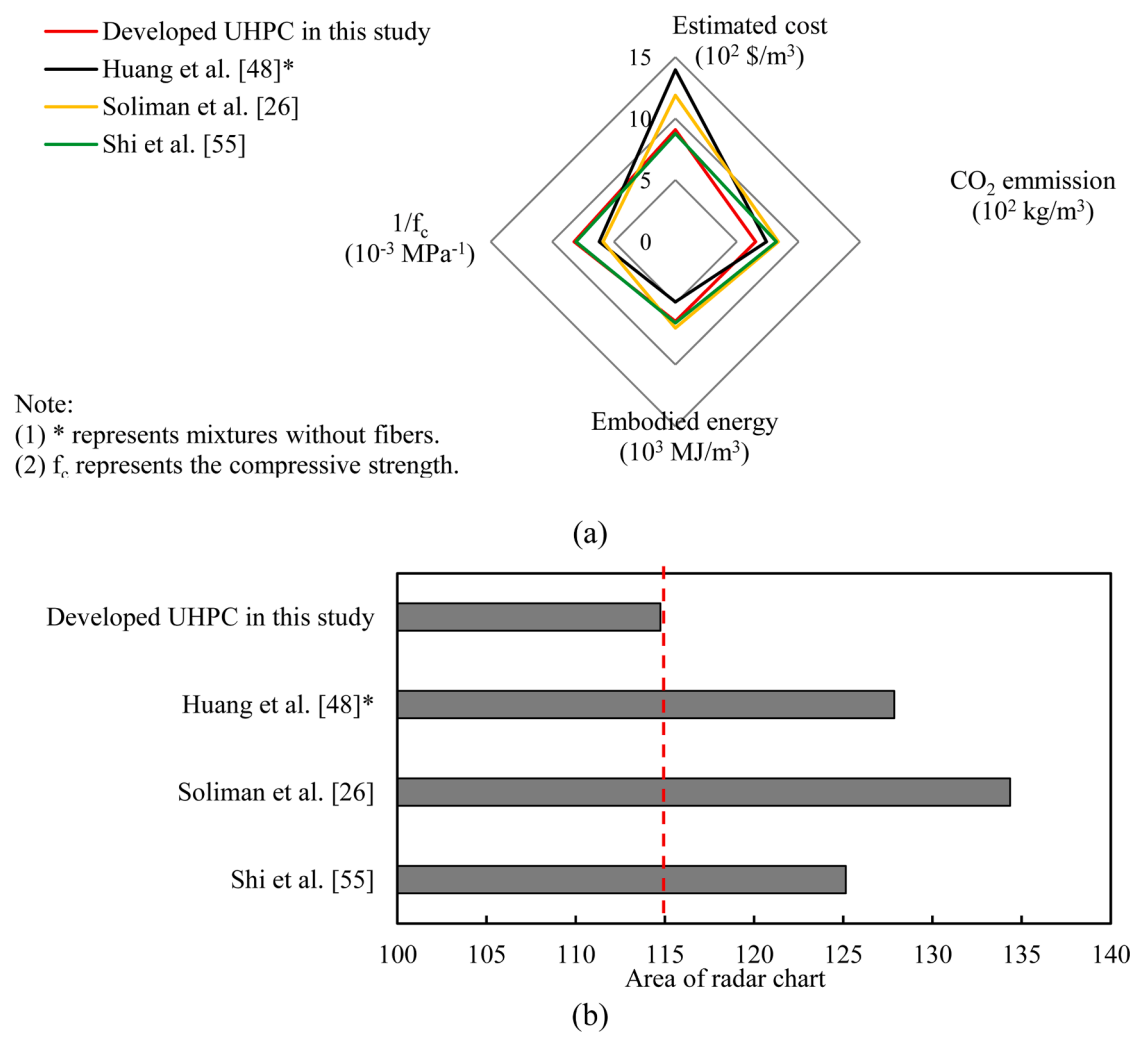


Fig. 5. Results of economic and environmental evaluation for different UHPC mixtures: (a) radar chart; and (b) summarized area of the radar chart.

control mixture, the use of OSFA and slag reduced the unit cost, and the combination use of OSFA, and slag reduced both the unit cost and strength-normalized cost. Currently, the proprietary UHPC product has a unit cost of about 2500 - 3000  $\mbox{$\rm m}^3$ , and its strength-normalized cost is about 16–20  $\mbox{$\rm m}^3$ /MPa. The unit cost of OSFA20SL40 is 909  $\mbox{$\rm m}^3$ , which is about 30% - 36% of the unit cost of the proprietary UHPC. The strength-normalized cost of OSFA20SL40 is 7.5  $\mbox{$\rm m}^3$ /MPa, which is about 38%–47% of the strength-normalized cost of the proprietary UHPC.

# 5.3. Carbon footprint

With the inventory data in Table B4, the carbon footprint of each mixture can be calculated using Eq. (3):

$$C = \sum_{i=1}^{n} c_i r_i \tag{3}$$

where C is the carbon footprint of a mixture;  $c_i$  is the unit carbon emission of the i th ingredient of the mixture (i=1,2,3,, n, and n=7), as listed in Table B4; and  $r_i$  is the mass of the i th ingredient of the mixture, as listed in Table 1.

According to Eq. (3), the unit carbon footprint of each mixture was calculated. With the compressive strength (MPa) of each mixture at 28 d, the strength-normalized carbon footprint (kg/m³/MPa) was calculated. Fig. A9 in Appendix A plots the results of the unit carbon footprint and

strength-normalized carbon footprint of the investigated mixtures. As the OSFA content increased from 0 to 30%, the unit carbon footprint was reduced from 1194 to 942 kg/m<sup>3</sup>, and the strength-normalized carbon footprint was increased from 11.4 kg/m<sup>3</sup>/MPa to 12.2 kg/m<sup>3</sup>/MPa, because the use of OSFA reduced the compressive strength. As the waterto-binder ratio decreased from 0.23 to 0.19, the unit carbon footprint was increased from 1028 kg/m3 to 1068 kg/m3, while the strengthnormalized carbon footprint was first reduced and then increased. OSFA20-21 achieved the lowest strength-normalized carbon footprint, because OSFA20-21 had a high compressive strength. As the slag content increased from 0 to 60%, the unit carbon footprint was reduced from 1028 kg/m<sup>3</sup> to 460 kg/m<sup>3</sup>, and the strength-normalized carbon footprint was reduced from 12.5 kg/m<sup>3</sup>/MPa to 4.2 kg/m<sup>3</sup>/MPa. Compared with the control mixture, the use of OSFA and slag reduced the unit carbon footprint, and combination use of OSFA, and slag reduced both unit carbon footprint and strength-normalized carbon footprint. For the optimal UHPC mixture is OSFA20SL40, the unit carbon footprint and strength-normalized carbon footprint are 687 kg/m<sup>3</sup> and 5.4 kg/m<sup>3</sup>/MPa, respectively.

### 5.4. Embodied energy

With the inventory data in Table B4, the embodied energy of each mixture can be calculated using Eq. (3):

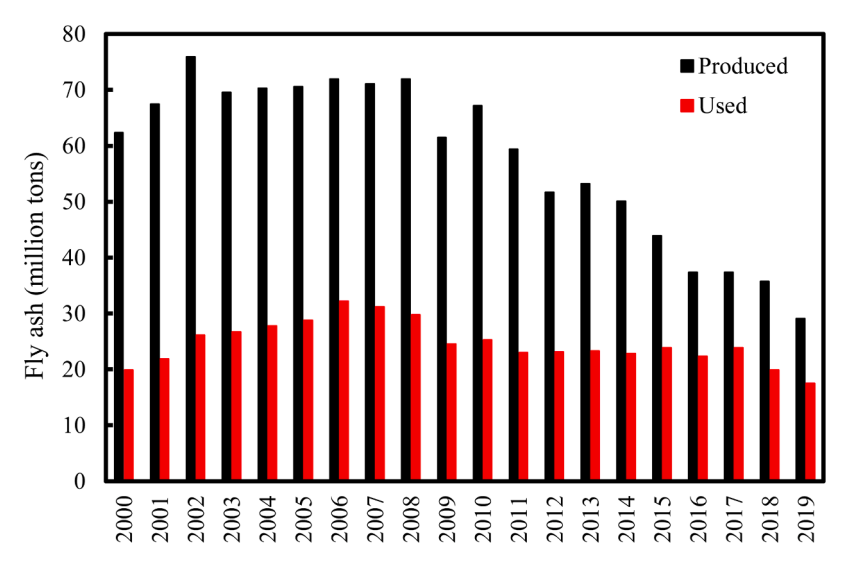


Fig. A1. Statistics of production and consumption of fly ash from 2000 to 2019 in the U.S. (ASTM C618-19 Standard 2019).

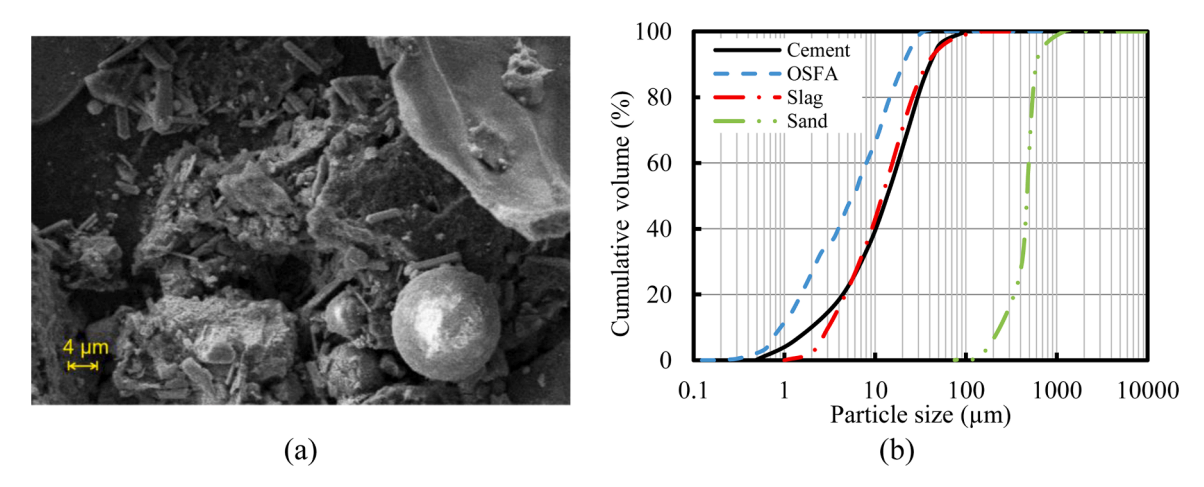


Fig. A2. Characterization of morphology and particle size of off-specification fly ash: (a) SEM image; and (b) particle size gradation.

$$E = \sum_{i=1}^{n} e_i r_i \tag{4}$$

where E is the embodied energy of a mixture;  $e_i$  is the unit embodied energy of the i th ingredient of the mixture (i=1,2,3,...,n, and n=7), as listed in Table B4; and  $r_i$  is the mass of the i th ingredient of the mixture, as listed in Table 1.

According to Eq. (4), the unit embodied energy of each mixture was calculated. With the compressive strength (MPa) of each mixture at 28 d, the strength-normalized embodied energy (MJ/m<sup>3</sup>/MPa) was calculated. Fig. A10 in Appendix A plots the results of embodied energy and strength-normalized embodied energy of the investigated mixtures. As the OSFA content increased from 0 to 30%, the embodied energy was reduced from  $8983 \text{ MJ/m}^3$  to  $7532 \text{ MJ/m}^3$ , and the strength-normalized embodied energy was increased from 85.7  $\mathrm{MJ/m^3/MPa}$  to 97.8  $\mathrm{MJ/m^3/MPa}$ MPa, because the use of OSFA reduced the compressive strength. As the water-to-binder ratio decreased from 0.23 to 0.19, the embodied energy was increased from 8029 MJ/m3 to 8356 MJ/m3, while the strengthnormalized embodied energy was first reduced and then increased. OSFA20-21 achieved the lowest strength-normalized embodied energy, because OSFA20-21 had a high compressive strength. As the slag content increased from 0 to 60%, the embodied energy was reduced from 8029 MJ/m<sup>3</sup> to 5696 MJ/m<sup>3</sup>, and the strength-normalized embodied energy was reduced from 97.5 MJ/m<sup>3</sup>/MPa to 52.2 MJ/m<sup>3</sup>/MPa.

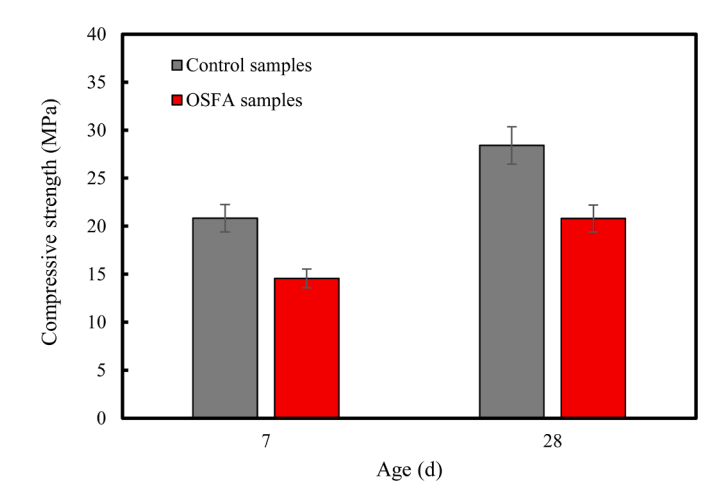


Fig. A3. Results of the strength activity indices of the control samples and OSFA samples.

Compared with the control mixture, the use of OSFA and slag reduced the embodied energy, and the combination use of OSFA, and slag reduced both the embodied energy and strength-normalized embodied

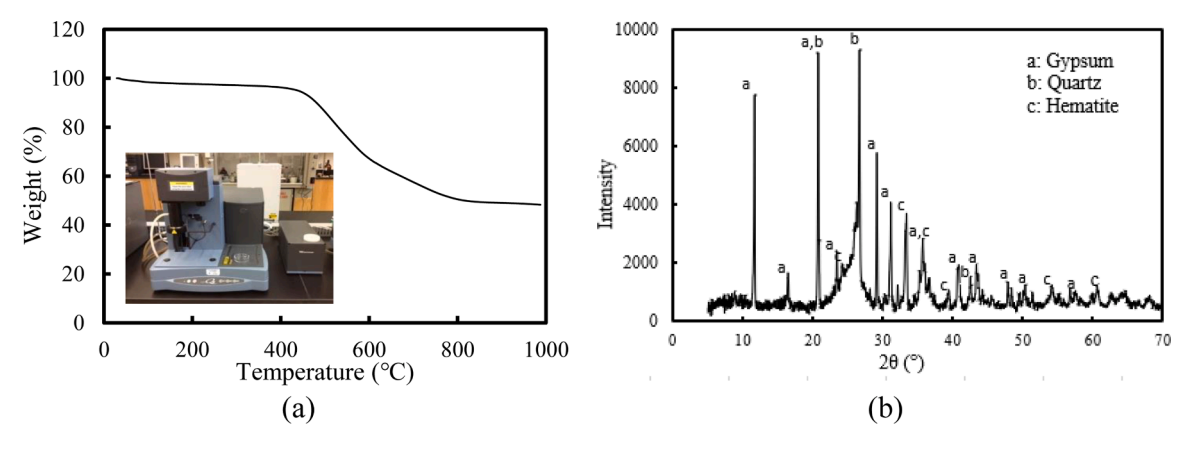


Fig. A4. Characterization of the investigated OSFA: (a) TGA result; and (b) XRD result.

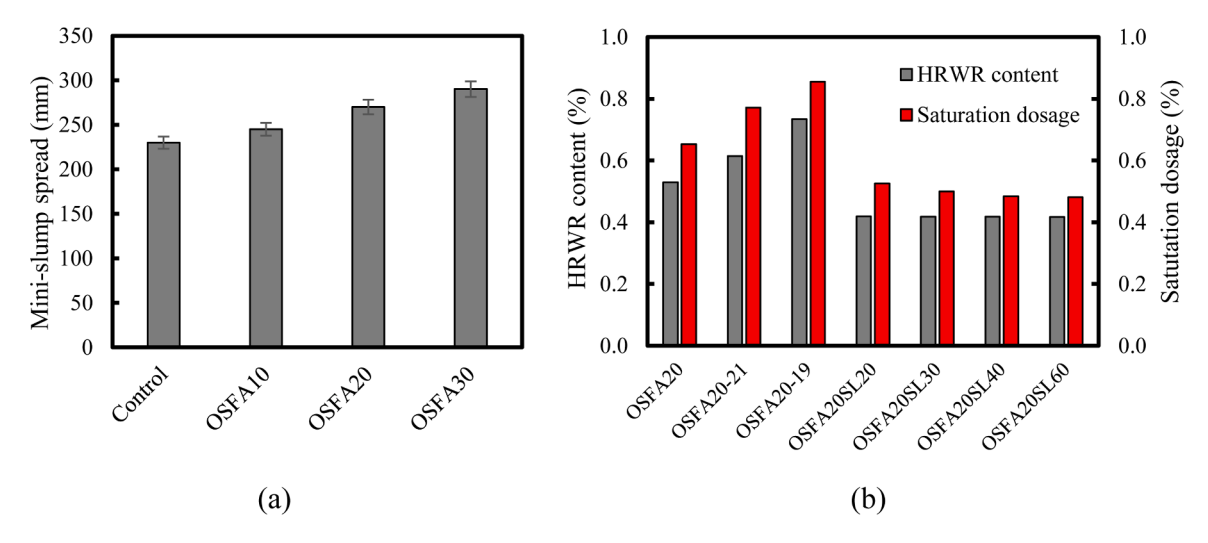


Fig. A5. Flowability results: (a) mini-slump spread of mixtures with different OSFA contents; and (b) HRWR demand. Note: HRWR content is fixed in (a), and the mini-slump spread is fixed in (b).

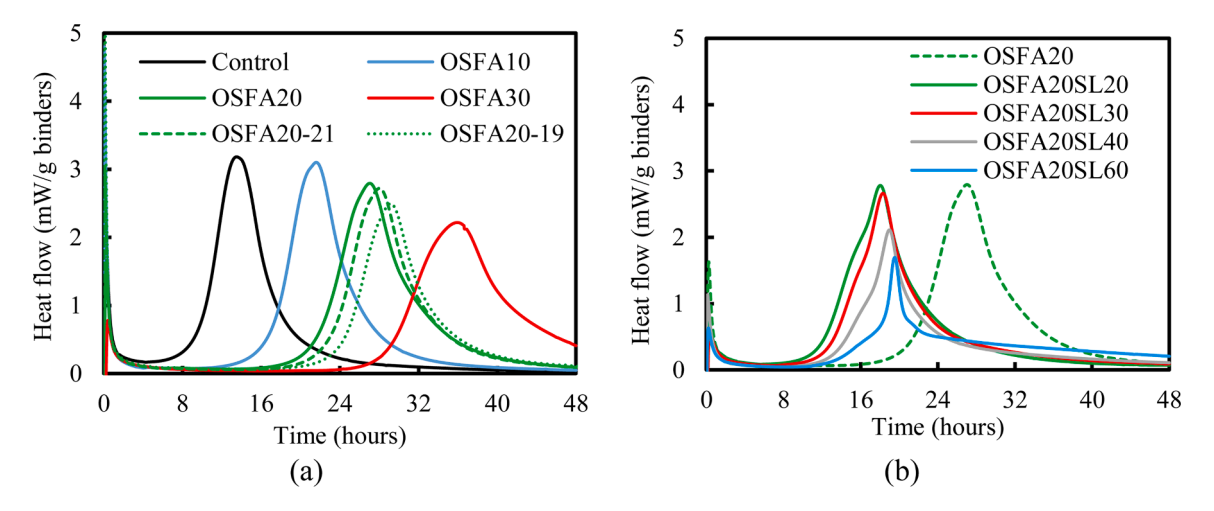


Fig. A6. Hydration heat results: (a) effects of OSFA content and water-to-binder ratio; and (b) effect of slag content.

energy. The optimal UHPC mixture in this study is OSFA20SL40. The embodied energy and strength-normalized embodied energy are  $6471 \text{ MJ/m}^3$  and  $53.3 \text{ MJ/m}^3$ /MPa, respectively.

## 5.5. Comparison with other UHPC mixtures

In recent years, development of UHPC mixture mainly focused on reducing the material cost,  $\rm CO_2$  emission, and embodied energy without mitigating the mechanical properties. In general, UHPC mixtures with

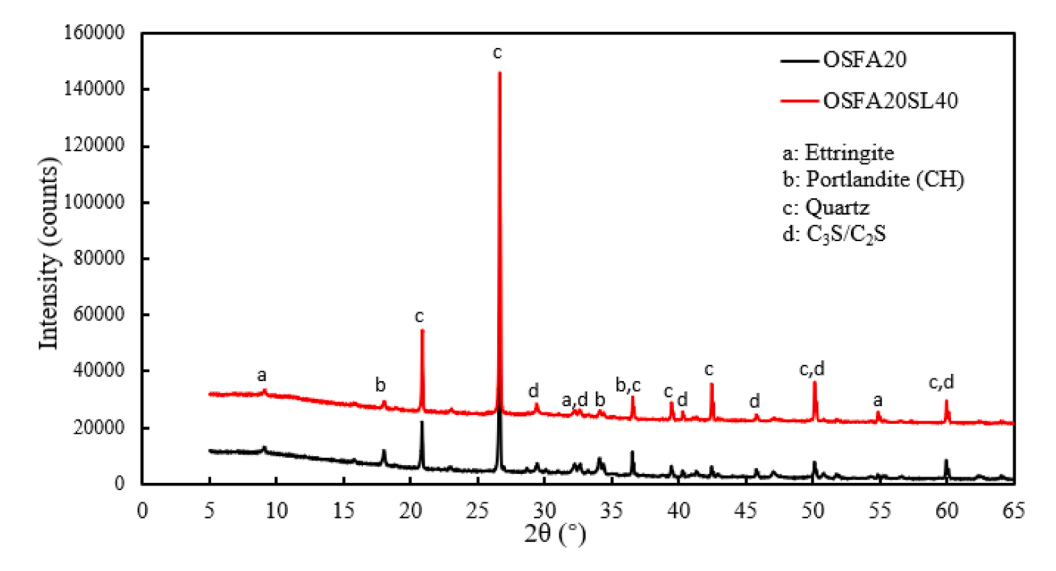


Fig. A7. Results of the XRD tests of mixtures OSFA20 and OSFA20SL40 (20 from 5  $^{\circ}$  to 65  $^{\circ}$ ).

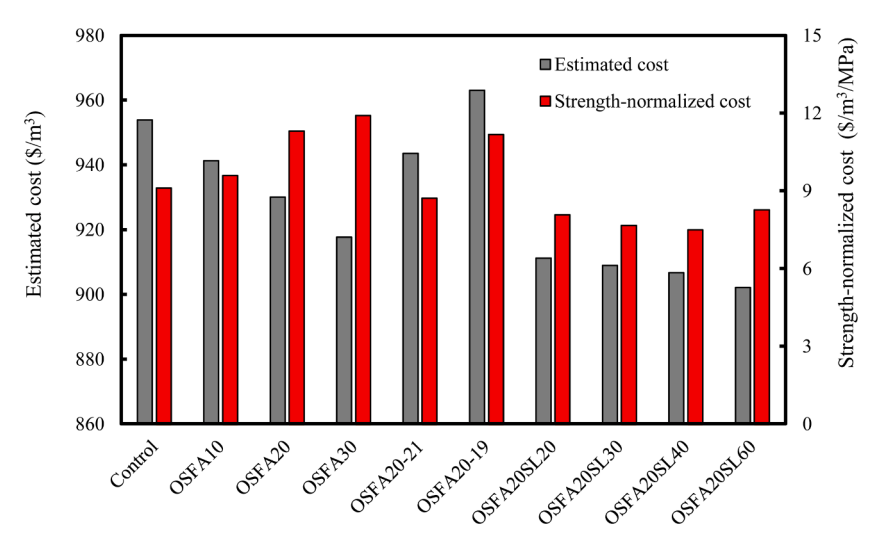


Fig. A8. Results of the unit cost and strength-normalized cost of the investigated mixtures.

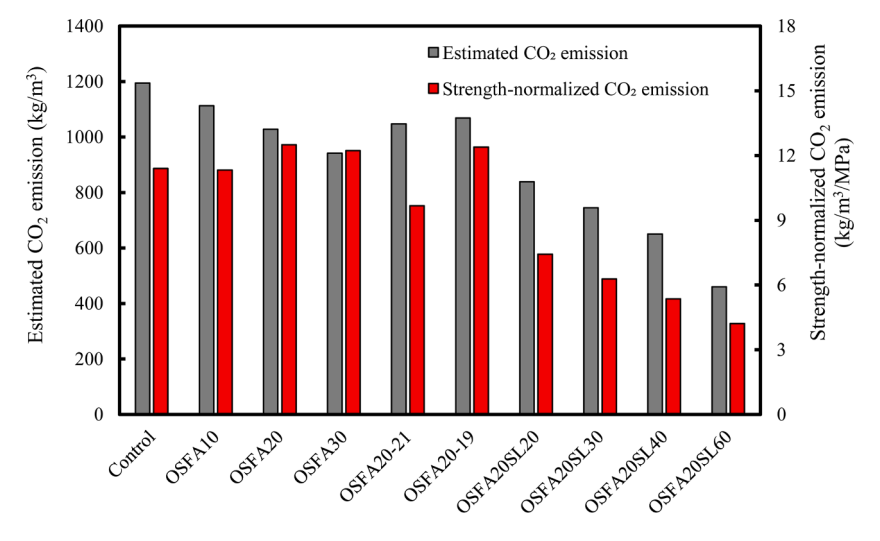


Fig. A9. Results of the unit carbon footprint and strength-normalized carbon footprint of the investigated mixtures.

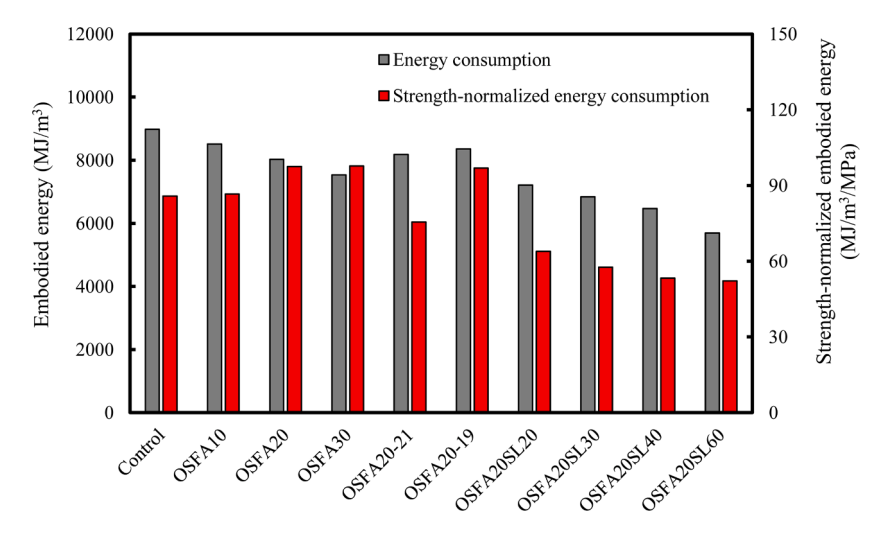


Fig. A10. Results of the energy consumption and strength-normalized energy consumption of the investigated mixtures.

higher mechanical performance have higher material cost,  $CO_2$  emission, and embodied energy. Fig. 5(a) plots the estimated cost,  $CO_2$  emission, embodied energy, and compressive strength of the optimized UHPC mixture OSFA20SL40 and other types of green UHPC mixtures reported in references (Edwin et al., 2016; Huang et al., 2017; Shi et al., 2019). In the radar chart, a small area represents good overall performance with low cost,  $CO_2$  emission, and embodied energy, as well as high compressive strength. Fig. 5(b) compares the areas of radar charts of different UHPC mixtures. The UHPC mixture developed in this study shows the smallest area and thus the best performance.

### 6. Conclusions

This study provides a new pathway for recycling OSFA and development of cost-effective UHPC through investigating the feasibility and benefits of using OSFA in preparing UHPC and developing promising UHPC mixtures. Comprehensive experiments were conducted to evaluate the effects of OSFA content, water-to-binder ratio, and slag content on the fresh and hardened properties as well as leachability of UHPC. The underlying mechanisms were investigated through isothermal calorimetry, thermal gravimetry, and X-ray diffraction. The economic and environmental evaluations of using OSFA in preparing UHPC showed the great benefits in environmental conservation and waste resource recycling. Based on the above investigations, the following conclusions are drawn:

- (1) Addition of OSFA improved the flowability of UHPC mixtures. As the OSFA content increased from 0 to 30%, the mini-slump spread was increased from 230 mm to 290 mm (by 26%). The improvement was attributed to the finer OSFA particles compared with cement.
- (2) Use of OSFA reduced the compressive strength, flexural strength, and toughness of UHPC because OSFA retarded hydration reactions. As the OSFA content increased from 0 to 30%, the compressive strength was reduced from 104.7 MPa to 77.1 MPa (by 26%), the flexural strength was reduced from 27.5 MPa and 17.6 MPa (by 36%), and the toughness was reduced from 7.8 kNmm to 5.0 kNmm (by 36%).
- (3) The use of slag suppressed the adverse effects of OSFA on the compressive strength, flexural strength, and toughness through promoting pozzolanic reactions. With a slag content of 40% by binder volume, the mixture achieved compressive strength, flexural strength, and toughness of 121.4 MPa, 27.1 MPa, and 7.3 kNmm.

- (4) The use of OSFA reduced the autogenous shrinkage of UHPC mixtures. As the OSFA content increased from 0 to 30%, the autogenous shrinkage decreased from 1089  $\mu\epsilon$  to 593  $\mu\epsilon$  (by 46%). With incorporation of slag at 60% by volume of binder, the autogenous shrinkage was 662  $\mu\epsilon$ , which is reasonably low for UHPC mixtures.
- (5) Based on the life-cycle assessment of economic and environmental features of UHPC with OSFA, the developed UHPC mixtures demonstrated significant benefits from the perspective of sustainability and economy. With the optimal mixture with an OSFA content of 20% and slag content of 40%, the estimated life-cycle cost, carbon footprint, and embodied energy were reduced to 909 dollar/m3, 651 kg/m3, and 6471 MJ/m3. In addition, leaching of heavy metals from the UHPC mixtures is negligible.
- (6) Compared with other UHPC mixtures proposed in recent years, the developed UHPC mixture in this study, such as OSFA20SL40, shows great potential in developing green and cost-effective UHPC

### Credit author statement

Jiang Du: Data curation; Formal analysis; Investigation; Visualization; Writing - original draft. Zhuo Liu: Data curation; Validation; Writing - review & editing. Christos Christodoulatos: Writing – review & editing; Supervision. Matthew Conway: Funding acquisition; Resource; Supervision. Yi Bao: Conceptualization; Methodology; Supervision; Writing - review & editing. Weina Meng: Conceptualization; Project administration; Resources; Supervision; Funding acquisition; Writing - review & editing.

### **Declaration of Competing Interest**

The authors declare that they have no known competing financial interests or personal relationships that could have appeared to influence the work reported in this paper.

### Acknowledgement

This research was funded by National Science and Foundation (award number: CMMI-2046407) and the US Army Corps of Engineers Mobile District via SIA Solutions LLC Prime Contract No.: W91278–16-D-0007. The contents of this paper reflect the views of the authors and do not necessarily reflect the official views or policies of the sponsor. Certain commercial equipment, instruments, or materials are identified in this paper to specify the experimental procedure. Such identification

is not intended to imply recommendation or endorsement nor to imply the materials or equipment are the best available for the purpose.

### **Appendix**

Two appendices are included to provide supplementary information for the main body of the paper. Specifically, Appendix A presents the supplementary figures. Appendix B presents the supplementary tables.

### References

- Aaleti, S., Sritharan, S., and Abu-Hawash, A. Innovative UHPC-normal concrete composite bridge deck. in Proceedings of the RILEM-fib-AFGC International Symposium on Ultra-High Performance Reinforced Concrete, Bagneux, France. 2013.
- Alahmari, T., Kennedy, C., Cuaron, A., Weldon, B., Jauregui, D, 2019. Field testing of a prestressed concrete bridge with high performance and locally developed ultra-high performance girders. Front. Built Environ. 5, 114.
- ASTM C109 /C109M-20b, 2020. Standard test method for compressive strength of hydraulic cement mortars. ASTM International.
- ASTM C1609 /C1609M-19a, 2019. Standard test method for flexural performance of fiber-reinforced concrete. ASTM International.
- ASTM C1698-19, 2019. Standard Test Method for Autogenous Strain of Cement Paste and Mortar. ASTM International.
- ASTM C230, 2021. Standard Specification for Flow Table For Use in Tests of Hydraulic Cement. ASTM International.
- ASTM C618-19 Standard, 2019. Specification for coal fly ash and raw or calcined natural pozzolan for use in concrete. ASTM International.
- ASTM C618-19, Standard specification for coal fly ash and raw or calcined natural pozzolan for use in concrete. 2019, ASTM International.
- Berndt, M.L., 2009. Properties of sustainable concrete containing fly ash, slag and recycled concrete aggregate. Constr. Build. Mater. 23 (7), 2606-2613.
- Brouwers, H., 2004. The work of Powers and Brownyard revisited: part 1. Cem. Concr. Res. 34 (9), 1697–1716.
- Brouwers, H., 2005. The work of Powers and Brownyard revisited: part 2. Cem. Concr. Res. 35 (10), 1922-1936.
- Cetin, B., Aydilek, A.H., Guney, Y, 2012. Leaching of trace metals from high carbon fly ash stabilized highway base layers. Resour. Conserv. Recycl. 58, 8-17.
- Chiaia, B., Fantilli, A.P., Guerini, A., Volpatti, G., Zampini, D, 2014. Eco-mechanical index for structural concrete. Constr. Build. Mater. 67, 386-392.
- Coal Combustion Products Production & Use Reports. 2019, American coal ash association.
- Colangelo, F., Navarro, T.G., Farina, I., Petrillo, A., 2020. Comparative LCA of concrete with recycled aggregates: a circular economy mindset in Europe. Int. J. LCA 25 (9), 1790-1804.
- De Medeiros, M.H.F., Raisdorfer, J.W., Hoppe Filho, J., Medeiros-Junior, R.A., 2017. Partial replacement and addition of fly ash in Portland cement: influences on carbonation and alkaline reserve. J. Build. Rehabil. 2 (1), 4.
- Donatello, S., Tyrer, M., Cheeseman, C., 2010. Comparison of test methods to assess pozzolanic activity. Cem. Concr. Comp. 32 (2), 121-127.
- Du, J., Meng, W., Khayat, K.H., Bao, Y., Guo, P., Lyu, Z., Abu-obeidah, A., Nassif, H., Wang, H, 2021. New development of ultra-high-performance concrete (UHPC). Compos.Part B, 109220.
- Edwin, R.S., De Schepper, M., Gruyaert, E., De Belie, N., 2016. Effect of secondary copper slag as cementitious material in ultra-high performance mortar. Constr. Build. Mater. 119. 31-44
- EPA, U., 1992, Method 1311 Toxicity characteristic Leaching Procedure (TCLP), Agency EP, editor. Washington DC, USA 1992.
- Falmata, A., Sulaiman, A., Mohamed, R., Shettima, A, 2020. Mechanical properties of self-compacting high-performance concrete with fly ash and silica fume. SN Appl. Sci. 2 (1), 1-11.
- Ferraz, E., Andrejkovičová, S., Hajjaji, W., Velosa, A.L., Silva, A.S., Rocha, F., 2015. Pozzolanic activity of metakaolins by the French Standard of the modified Chapelle Test: a direct methodology. Acta Geodyn. et Geomater 12 (3), 289-298.
- Fly ash facts for highway engineers, 2003. American coal ash association, US department of transportation. Federal Highway Administration.
- Freeman, E., Gao, Y.M., Hurt, R., Suuberg, E., 1997. Interactions of carbon-containing fly ash with commercial air-entraining admixtures for concrete. Fuel 76 (8), 761-765.
- Ghafari, E., Ghahari, S.A., Costa, H., Júlio, E., Portugal, A., Durães, L., 2016. Effect of supplementary cementitious materials on autogenous shrinkage of ultra-high performance concrete. Constr. Build. Mater. 127, 43–48.
- Graybeal, B.A., Characterization of the behavior of ultra-high performance concrete (Doctoral dissertation), 2005.

- Graybeal, B.A., 2010. Field-cast UHPC connections for modular bridge deck elements. United States. Federal Highway Administration. Office of Infrastructure Research and Development.
- Graybeal, B.A., 2012. Ultra-high performance concrete composite connections for precast concrete bridge decks. United States Federal Highway Administration. Office of Infrastructure Research and Development.
- Hill, R.L., Sarkar, S.L., Rathbone, R.F., Hower, J.C., 1997. An examination of fly ash carbon and its interactions with air entraining agent. Cem. Concr. Res. 27 (2),
- Holt, E., Leivo, M., 2004. Cracking risks associated with early age shrinkage. Cem. Concr. Comp. 26 (5), 521-530.
- Huang, W., Kazemi-Kamyab, H., Sun, W., Scrivener, K., 2017. Effect of cement substitution by limestone on the hydration and microstructural development of ultra-high performance concrete (UHPC). Cem. Concr. Comp. 77, 86-101.
- Li, P., Yu, Q., Brouwers, H., 2017. Effect of PCE-type superplasticizer on early-age behaviour of ultra-high performance concrete (UHPC). Constr. Build. Mater 153,
- Lim, S., Lee, W., Choo, H., Lee, C., 2017. Utilization of high carbon fly ash and copper slag in electrically conductive controlled low strength material. Constr. Build. Mater. 157, 42-50,
- Lo, T.Y., Cui, H., Memon, S.A., Noguchi, T., 2016. Manufacturing of sintered lightweight aggregate using high-carbon fly ash and its effect on the mechanical properties and microstructure of concrete. J. Clean. Prod. 112, 753-762.
- Long, G., Gao, Y., Xie, Y., 2015. Designing more sustainable and greener self-compacting concrete. Constr. Build. Mater. 84, 301-306.
- Meng, W., Khayat, K.H, 2017. Improving flexural performance of ultra-high-performance concrete by rheology control of suspending mortar. Compos.Part B 117, 26-34.
- Meng, W., Valipour, M., Khayat, K.H., 2017. Optimization and performance of costeffective ultra-high performance concrete. Mater. Struct. 50 (1), 29.
- Naik, T.R., Kumar, R., Ramme, B.W., Kraus, R.N., 2010. Effect of high-carbon fly ash on the electrical resistivity of fly ash concrete containing carbon fibers. In: Proceedings of the Conference on Sustainable Construction Materials and Technologies, Italy.
- Qi, J., Bao, Y., Wang, J., Li, L., Li, W., 2019. Flexural behavior of an innovative dovetail UHPC joint in composite bridges under negative bending moment. Eng. Struct. 200,
- Ramme, B.W. and Tharaniyil, M.P. Coal combustion products utilization handbook 2014. Scrivener, K., Snellings, R., Lothenbach, B., 2018. A Practical Guide to Microstructural Analysis of Cementitious Materials. CRC Press.
- Sevim, U.K., Bilgic, H.H., Cansiz, O.F., Ozturk, M., Atis, C.D., 2021. Compressive strength prediction models for cementitious composites with fly ash using machine learning techniques. Constr. Build. Mater. 271, 121584.
- Shi, Y., Long, G., Ma, C., Xie, Y., He, J., 2019. Design and preparation of ultra-high
- performance concrete with low environmental impact. J. Clean. Prod. 214, 633–643. Soliman, N., Tagnit-Hamou, A., 2016. Development of ultra-high-performance concrete using glass powder-Towards ecofriendly concrete. Constr. Build. Mater. 125, 600-612.
- Soliman, N., Tagnit-Hamou, A., 2017. Partial substitution of silica fume with fine glass powder in UHPC: filling the micro gap. Constr. Build. Mater. 139, 374-383.
- Teng, L., Meng, W., Khayat, K.H., 2020. Rheology control of ultra-high-performance concrete made with different fiber contents. Cem. Concr. Res 138, 106222.
- Van der Merwe, E., Strydom, C., Potgieter, J., 1999. Thermogravimetric analysis of the reaction between carbon and CaSO4•2H2O, gypsum and phosphogypsum in an inert atmosphere. Thermochim. Acta 340, 431-437.
- Verger-Leboeuf, S., Charron, J.P., Massicotte, B., 2017. Design and behavior of UHPFRC field-cast transverse connections between precast bridge deck elements. J. Bridge Eng 22 (7), 04017031.
- Voort, T.V., Suleiman, M.T., Sritharan, S., 2008. Design and performance verification of ultra-high performance concrete piles for deep foundations. IOWA State University, Center for Transportation Research and Education.
- Wen, H., Baugh, J., Edil, T., Wang, J, 2011. Cementitious high-carbon fly ash used to stabilize recycled pavement materials as base course. Transp. Res. Rec. 2204 (1), 110-113.
- Wille, K., Boisvert-Cotulio, C., 2015. Material efficiency in the design of ultra-high performance concrete. Constr. Build. Mater. 86, 33-43.
- Xie, J., Fu, O., Yan, J.B, 2019. Compressive behaviour of stub concrete column strengthened with ultra-high performance concrete jacket. Constr. Build. Mater. 204, 643-658.
- Yang, L., Shi, C., Wu, Z, 2019. Mitigation techniques for autogenous shrinkage of ultrahigh-performance concrete-a review. Compos.Part B 178, 107456.
- Yoo, D.Y., Park, J.J., Kim, S.W., Yoon, Y.S., 2014. Influence of reinforcing bar type on autogenous shrinkage stress and bond behavior of ultra high performance fiber reinforced concrete. Cem. Concr. Comp. 48, 150-161.
- Yu, R., Spiesz, P., Brouwers, H., 2015. Development of an eco-friendly ultra-high performance concrete (UHPC) with efficient cement and mineral admixtures uses. Cem. Concr. Comp. 55, 383-394.